Chiral interaction in double-wall carbon nanotubes: Simple rules deduced from a large sampling of tubes

D. Vardanega, F. Picaud, and C. Girardet[a)]
Laboratoire de Physique Moléculaire, UMR CNRS 6624, Faculté des Sciences, La Bouloie, Université de Franche-Comté, F25030 Besançon Cedex, France

(Received 15 December 2009; accepted 26 February 2010; published online 29 March 2010)

We study a large sampling of chiral double-wall carbon nanotubes to propose simple formula describing the dependence of the interwall energy, the chiral discrimination energy, and the radial breathing mode frequencies as a function of the main characteristics of the tubes, i.e., their radius, length and chiral angle. It is shown that tube pairs with the same handedness are more stable than enantiomeric pairs, and this discrimination, though small, mainly occurs in the first step of the growth of an inner tube inside an outer one. Chiral splittings of the breathing mode frequencies for the two DWCNT diastereoisomers $(n_i,m_i)@(n_o,m_o)$ and $(m_i,n_i)@(n_o,m_o)$ can reach a few wave numbers. © *2010 American Institute of Physics*. [doi:10.1063/1.3366688]

I. INTRODUCTION

The structure of single-wall carbon nanotubes (SWCNTs) is defined[1] by the length L, the radius R, and the chiral angle α describing the helical twist of the rolled-up graphene sheet. With the exception of armchair and zig-zag tubes, all the other tubes are chiral, i.e., the tubes of right (r)- and left (l)-handed helicities are enantiomers of each other. The geometry of the CNT can also be described[2] by reference to the graphene sheet using two integers (n,m) defining any lattice point from the unit cell vectors of the sheet. Chirality can then be viewed through the reverse nomenclature (n,m) for the l-handed and (m,n) for the r-handed species. Other terminologies have also been proposed in the literature.[3]

Sorting the CNTs from their structural properties (L,R,α) has been an experimental challenge which has drawn considerable attention over the past few years.[4–8] Many separation mechanisms have been devised, with special emphasis to the control of chirality and enantiomeric detection.[7,9–11] At the frontier between single wall and multiwall nanotubes, double-wall carbon nanotubes (DWCNTs) have been considered as ideal, having the thinnest graphite structure with excellent graphitization,[11] to study how the correlation between the two rolled-up graphene layers influences the relationship between the structural and electromechanical properties of the tubes. Selective syntheses of DWCNTs have been largely reported,[12–14] and among them, let us cite the peapod growth technique[15] which provides tubes of nearly perfect purity with generally small diameters.[16,17] The determination of the chirality of the two constituent tubes has been tentatively performed using Raman spectroscopy,[18] electron diffraction,[19] transmission electron microscopy,[20] and coupling scanning tunneling microscopy and spectroscopy experiments.[21] In a general way, from a reasonably small sampling of DWCNTs, it was concluded that no (or very small) correlation exists between the chiral angles of the inner and outer tubes and the distribution of the nanotubes. Such a result corroborated previous theoretical results[22] devoted to the calculation of the most stable structures of DWCNTs described by the four integer numbers $(n_i,m_i)@(n_o,m_o)$, where i refers to the inner tube and o refers to the outer one. However, from the assignment of DWCNT chiralities using radial breathing modes, compared to experimental data,[23] it has been suggested[24] that the effect of chirality, though small, should not be neglected to interpret the complete splitting of the components in the high resolution Raman response of the inner tubes.

The handedness relationship between the two layers in nested DWCNTs was investigated for the first time in Ref. 25. Handedness measurements of 18 chiral DWCNTs lead to the conclusion that some interaction may have been exerted during the simultaneous growth of the tubes to prefer the same handedness for the inner and outer tubes. Besides, chiral angles and tube radii were carefully measured over a sampling of 140 isolated $(n_i,m_i)@(n_o,m_o)$ DWCNTs.[20] The distribution of the tube number as a function of the interwall distance ΔR and radii (R_i,R_o) and as a function of the chiral angles (α_i,α_o) was determined for small and large radii. It showed a different tendency, with chiral angles approaching $\pi/6$ for radii less than 15 Å, while the distribution was much wider for larger (R_i,R_o) values.

Calculations of stable structures of a set of DWCNTs have been carried out, including achiral species (armchair and zig-zag), based on a Lennard-Jones potential between carbon atoms belonging to the two layers.[22] Information on the interlayer spacing ΔR and on the adiabatic potential shape has been obtained, showing a flat potential shape for ΔR values ranging between 3.3 and 3.5 Å. The same type of potential was used[26] to propose a classification scheme for DWCNTs based on their symmetry properties and to calculate the rotation and translation barriers of the inner tube with respect to the outer one. An analytical form of the interaction potential between the two concentric tubes, deduced from a 6-exp. binary potential, was expressed[27] as a

[a)]Electronic mail: claude.girardet@univ-fcomte.fr.

function of the parameters ΔR, α_i, and α_o (or ΔR and $\Delta\alpha = \alpha_i - \alpha_o$). This form was successfully applied[28] to the determination of the stable structure of seven DWCNTs identified in transmission electron microscopy experiments.[29]

In fact, it is still unclear as to whether the relative handedness of the two tubes can influence the structural and, as a consequence, the electromechanical properties of DWCNTs. It seems therefore crucial to have some simple rules on the behavior of the interaction energy between the two tubes depending on their mutual handedness and on the relationship between this energy and interwall distance ΔR, radii R_i and R_o, lengths L_i and L_o, and tube helicities α_i, α_o, and $\Delta\alpha$, using a very large sampling of chiral tubes. This can be made based on a simple potential, even if very recent progresses[30] in the implementation of van der Waals density functional theory for CNTs could lead in the future to appreciably reduced computational times.

In Sec. II, we introduce the background to calculate the interaction energy and related quantities depending on the relative geometry of the two tubes in a DWCNT. Section III is devoted to the presentation of the results and of the rules deduced from the sampling of about 3000 chiral DWCNTs (the two tubes being chiral). The dependence of the interaction with the mutual chirality of the two tubes, and the discrimination energy between two l-handed tubes (or in equivalent way between two r-handed tubes) and one l- and the other r-handed tube, is carefully analyzed. We also examine the influence of the chirality on the resonance frequencies of the radial breathing modes, as these frequencies are sensitive tests of the DWCNT structure. We discuss in Sec. IV the consequences of these results on the distribution of DWCNTs using a simple model that mimics the growth of a tube in an outer one, and we show that the frequency splitting of the breathing modes is influenced by the handedness of the two tubes.

II. BACKGROUND

DWCNTs are characterized by the four integers n_i, m_i, n_o, and m_o, which define the period B, the radius R, and the chiral angle α of each i or o tube. For a SWCNT (n,m), these quantities are given as

$$B = \frac{3\mathrm{d_{CC}}}{\mathrm{GCD}(n,m)}\sqrt{n^2+m^2+nm}, \tag{1}$$

$$R = \frac{\sqrt{3}\mathrm{d_{CC}}}{2\pi}\sqrt{n^2+m^2+nm}, \tag{2}$$

$$\alpha = \arccos\left[\frac{2m+n}{2\sqrt{n^2+m^2+nm}}\right], \tag{3}$$

where $\mathrm{d_{CC}}=1.42$ Å is the carbon-carbon bond length in a tube, and $\mathrm{GCD}(n,m)$ mean the greatest common divisor of n and m.

The interaction between the two tubes i and o with radii R_i and R_o, respectively, is a function of the distance $d_{j_i j_o}$ between the j_ith atom of the inner tube and the j_oth atom of the outer one. Using a helicoidal description of carbon atom arrangement in each tube, which is consistent with the chirality (Fig. 1), the jth atom can be characterized by the triplet of integer numbers (s,l,h), where s refers to the two atoms in the unit cell along the helix $(s=0,1)$, l is the cell number $[l=0,\ldots,N_C-1=2(n^2+m^2+nm)/(|m-n|\mathrm{GCD}(n,m))-1]$, and h is the helix number required to account for all the carbon atoms of the chiral tube $(h=0,\ldots,|m-n|-1)$. The square of the distance $d_{j_i j_o}$ is expressed as

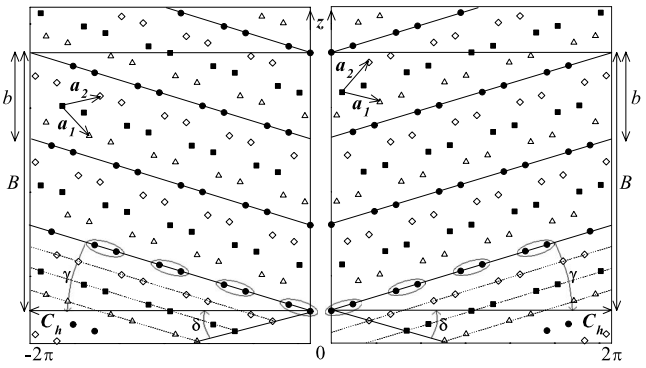

FIG. 1. Geometry of left-handed (2,6) and right-handed (6,2) SWCNT, respectively, at the left and right parts. **z** means the nanotube axis and $\mathbf{C_h} = n\mathbf{a_1} + m\mathbf{a_2}$ is the chiral vector, where $\mathbf{a_1}$ and $\mathbf{a_2}$ are the unit vectors defining the cell on a graphene sheet. b is the helix pitch and B is the period of the CNT. Angle $\gamma = \arccos(\sqrt{3}(n+m)/(2\sqrt{n^2+m^2+nm}))$ defines the helicity of the tube and it is equal to $(\pi/6-\alpha)$ or $(\alpha-\pi/6)$ depending on the handedness of the tube, where α is the chiral angle. Angle δ is equal to $\arccos((2m+n)/(2\sqrt{n^2+m^2+nm}))$ and it corresponds to α or $(\pi/3-\alpha)$. Circles, triangles, squares, and diamonds define the atom arrangement on the various helices in the tubes.

$$\begin{aligned} d_{j_i j_o}^2 = {} & R_i^2 + R_o^2 \\ & - 2R_iR_o\cos\left(\pi\left[\frac{(3l_i+s_i+h_i)(n_i+m_i)+m_ih_i}{n_i^2+m_i^2+n_im_i}\right.\right. \\ & \left.\left. - \frac{(3l_o+s_o+h_o)(n_o+m_o)+m_oh_o}{n_o^2+m_o^2+n_om_o}\right] - \theta\right) \\ & + \frac{\mathrm{d_{CC}^2}}{4}\left(\frac{(3l_i+s_i)(n_i+m_i)-3m_ih_i}{\sqrt{n_i^2+m_i^2+n_im_i}}\right. \\ & \left. - \frac{(3l_o+s_o)(n_o+m_o)-3m_oh_o}{\sqrt{n_o^2+m_o^2+n_om_o}} - z\right)^2. \end{aligned} \tag{4}$$

The coordinates θ and z define the position of the origin atom in the first helix $(h_o=0)$ of the outer tube with respect to the position of the origin atom in the first helix $(h_i=0)$ of the inner tube (Fig. 1). The interaction potential between two perfect (no defect, no deformation) concentric tubes is written as

$$V = \sum_{s_i,l_i,h_i}\sum_{s_o,l_o,h_o}\sum_{k=6,12}(-)^{k/2}\frac{C_k}{d_{j_ij_o}^k}, \tag{5}$$

where $\mathrm{C_6}=4\epsilon\sigma^6$ and $\mathrm{C_{12}}=4\epsilon\sigma^{12}$ are the Lennard-Jones coefficients between two carbon atoms. This interaction V depends on the mutual handedness of the two tubes forming the DWCNT. Depending on whether the two tubes have the same or different handedness, we define the energy as

$$W^{ll} = V(n_i,m_i,n_o,m_o) \equiv W^{rr} = V(m_i,n_i,m_o,n_o) \quad (6)$$

or

$$W^{lr} = V(n_i,m_i,m_o,n_o) \equiv W^{rl} = V(m_i,n_i,n_o,m_o). \quad (7)$$

These two energies were minimized with respect to θ and z occurring in Eq. (4) for a very large sampling of DWCNTs. For the inner tube, the series $n_i=1,\ldots,12$ and $m_i=n_i+1,\ldots,120$ have been considered with outer tubes indices (n_o,m_o) obeying the condition [see Eq. (2)].

$$\Delta R_{\min} \leq \Delta R = R_o - R_i \leq \Delta R_{\max}. \quad (8)$$

The values of $\Delta R_{\min}$ and $\Delta R_{\max}$ which are reported in the literature depend, in fact, on the preparation and synthesis methods of the DWCNTs. Interwall distances were found to range between 3.2 (Ref. 24) and 4.2 Å (Ref. 18), while other recent experiments[20,31] pointed out interwall distances ranging between 3.4 and 3.8 Å with an average value of 3.58 Å. Therefore, this latter dispersion of values for ΔR was considered to define $\Delta R_{\min}$ and $\Delta R_{\max}$. Several tests have been made, which have shown that the chiral discrimination rapidly vanishes when the interwall distance increases, and, on the contrary, strongly increases when this distance is smaller than the equilibrium value. Since we were mainly interested by the determination of the maximum chiral discrimination energy between the two tubes at physically stable distances, we generally reduced the range from $\Delta R_{\min}=3.4$ Å and $\Delta R_{\max}=3.6$ Å, leading to a sampling of about 3000 tubes, although some smaller values of $\Delta R_{\min}$ were also discussed in the calculation of the breathing mode frequencies.

Since the energies W^{ll} and W^{rl} depend on the inner and outer tubes lengths, the calculations were carried out by considering that the lengths L_i and L_o are multiple of the periods B_i and B_o of the tubes. More precisely, the length of the outer tube was taken to be $L_o=B_o$, and, to eliminate side effects in the sum process of the binary interactions, the length of the inner tube was chosen to be a multiple of B_i such that $L_i > L_o+60$ Å, i.e., adding 30 Å at each side of the inner tube. Moreover, we have verified that, by changing L_o into $2L_o$ and extending the convergence criterium for L_i, the results were not modified.

Then the interaction energies W^{ll} and W^{rl} for the two diastereoisomers $(n_i,m_i)@(n_o,m_o)$ or (l,l) and $(m_i,n_i)@(n_o,m_o)$ or (r,l) were expressed per contact surface unit $(2\pi R_i L_o)$ and renamed as W_S^{ll} and W_S^{rl} (in meV Å^{-2}).[32] Their behavior in terms of n, m, R, and α was studied by defining the mean energy $\bar{W}_S$ for the two diastereoisomers,

$$\bar{W}_S = \tfrac{1}{2}(W_S^{ll} + W_S^{rl}), \quad (9)$$

and the chiral discrimination energy ΔW_S as

$$\Delta W_S = W_S^{ll} - W_S^{rl}. \quad (10)$$

The potential parameters $\epsilon=2.1$ meV and $\sigma=3.5$ Å were used.[33] Other values of ϵ and σ given in the literature[22,34] have also been tested, which give a slight shift of the interwall distance depending on the σ value, but without appreciably changing the results reported in the present paper.

No analytical expression for the interaction potential between two continuous helicoidal tubes is available up to date. However, the interaction between two continuous achiral tubes (cylindrical geometry) is known[35] and it can be written as

$$W_S^C = \frac{2.921}{2\pi R_i L_o d_{CC}^4}\left(\sum_{k=6,12}(-)^{k/2}C_k\sum_{p=1}^{2}N_k(x,y_p)\right), \quad (11)$$

where the functions N_k are defined in the Appendix in terms of the tube radii and lengths.

Although this continuum energy W_S^C cannot take into account of the chiral dependence of the tubes, its analytical form can be used as a valuable test to validate the behavior of the computed mean energy $\bar{W}_S$ and, in particular, the fit in terms of $\Delta R/R_i$.

Aside from the DWCNT energies $\bar{W}_S$ and ΔW_S, the frequencies of the radial breathing modes provide information on the two tubes' chirality. These frequencies can be analytically written by considering the tube walls as coupled oscillators[36] as

$$\omega_{\pm}^2 = \frac{\Omega_i^2+\Omega_o^2}{2} \pm \left[\frac{(\Omega_i^2+\Omega_o^2)^2}{4} + \frac{k_{Sio}^2}{m_S^2}\right]^{1/2}, \quad (12)$$

where Ω_i^2 and Ω_o^2 are the square frequencies of the interacting inner and outer tubes defined as

$$\Omega_{i,o}^2 = \left(\frac{\xi}{2R_{i,o}}\right)^2 + \frac{k_{Si,o}}{m_S}. \quad (13)$$

In Eqs. (12) and (13), we use the value $\xi=2243$ cm^{-1} Å given in Ref. 36 and we introduce the mass per contact surface unit as $m_S=m/2\pi R_i L_o=4.58$ amu Å^{-2}, where m defines the mass of a tube with radius R_i and length L_o. k_{Sio}, k_{Si}, and k_{So} are the force constants per contact surface unit, obtained as the second order derivatives of the tube-tube interactions W_S^{ll} or W_S^{rl} with respect to the tube radii. They have been calculated from Eq. (5) by deriving V with respect to the distance $d_{j_i j_o}$ and expressing the derivatives of $d_{j_i j_o}$ with respect to $R_{i,o}$. Note that $R_{i,o}$ are themselves functions of $n_{i,o}$ and $m_{i,o}$.

III. RESULTS

A. Mean interaction energy

Figure 2 displays the behavior of the mean energy $\bar{W}_S$ [Eq. (9)] as a function of ΔR for typical series of DWCNTs. The minimum is relatively flat, as shown in a previous paper,[22] where a random sampling of pairs $(n_i,m_i)@(n_o,m_o)$ were considered with the outer larger radius less than 10 Å. In the present paper, the (l,l)- and (r,l)-handed tubes were studied for the inner tube series (1,2), (1,3), and (1,6) with respective radii of 1.04, 1.14, and 2.57 Å, yielding minimum energy values equal to −33, −30, and −23 meV Å^{-2}, respectively. The energy corresponding to the series with an inner tube (3,4) and a radius of 2.38 Å was also drawn since

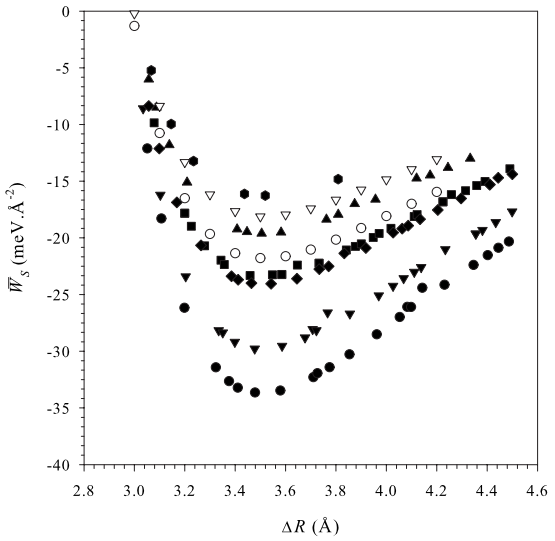

FIG. 2. Mean interaction energy $\bar{W}_S$ between the inner and outer tubes in various DWCNT series vs the interwall distance ΔR. The black symbols correspond to inner tubes (1,2) (circles), (1,3) (reverse triangles), (1,6) (squares), (3,4) (diamonds), (6,7) (triangles), and (4,27) (hexagons) having radii equal to 1.04, 1.41, 2.57, 2.38, 4.41, and 11.43 Å, respectively. The white symbols correspond to calculations performed within the continuum model for R_i=2.57 Å (circles) and R_i=5.00 Å (reverse triangles).

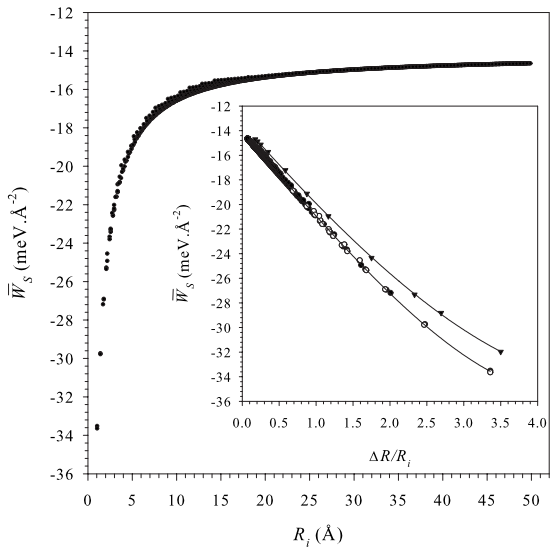

FIG. 3. Mean interaction energy $\bar{W}_S$ vs the inner tube radius R_i for a large sampling of DWCNTs (see the text). Inset: Same energy vs $\Delta R/R_i$ showing a quasilinear behavior. The black and white circles correspond to DWCNTs series with $\Delta n=0$ and $\Delta n \neq 0$, respectively. The broken line with black triangles is drawn using the continuum model.

it corresponds to the smallest tube experimentally identified.[29] Larger tubes in the series (6,7) and (4,27) with radii equal to 4.41 and 11.43 Å display minimum energy values which increase to −20 and −17 meV Å^{-2}. For comparison, the energy issued from the continuum model [Eq. (11)] was drawn for R_i=2.57 and 5.00 Å, i.e., values close to those of the (1,6) and (6,7) series, showing a very good agreement, within a systematic error less than 2 meV Å^{-2}. This agreement indicates that the continuum model applies very well and that chirality does not strongly influence the stability of the tubes in the DWCNTs, as already discussed.

Using the results in Fig. 2, we draw in Fig. 3 the mean energy $\bar{W}_S$ for the series (n_i,m_i) $(n_i=1,\ldots,12;\ m_i=n_i+1,\ldots,120)$ with outer tubes obeying the maximum stability of the DWCNTs, i.e., $3.4 \leq \Delta R \leq 3.6$ Å [Eq. (8)]. Within this constraint, the curve $\bar{W}_S(R_i)$ is fitted with a high accuracy to

$$\bar{W}_S = -14.13 - \frac{24.87}{R_i} + \frac{4.49}{R_i^2}. \tag{14}$$

The maximum is obtained for the smallest radius of the inner tubes $(n_i=1,\ m_i=2)$ with outer tubes $(n_o=1,\ m_o=11)$ and $(n_o=4,\ m_o=9)$. As the radius R_i increases, the energy $\bar{W}_S$ significantly increases to reach a nearly constant value. Shown in the inset (Fig. 3) is the dependence of $\bar{W}_S$ in terms of $\Delta R/R_i$, displaying a quasilinear behavior for $\Delta R/R_i$ values less than 1.6, i.e., values of $R_i \geq 2.2$ Å. The limit for very large R_i values can be compared to the energy between two graphene planes equal to −15.2 meV Å^{-2} and two graphite planes equal to −14.5 meV Å^{-2}. Note that the nonlinear part of the curve $\bar{W}_S(\Delta R/R_i)$ corresponds to very small inner tubes which have not been observed experimentally. In this inset, we have also drawn the behavior of W_S^C in the continuum model, which shows that the nonlinear part of the curve is typical of the small radius of the tube.

From Eq. (14) and using the relation

$$R_i\alpha_i \approx R_i \sin\alpha_i = \frac{3d_{CC}}{4\pi}n_i, \tag{15}$$

we can also express the behavior of $\bar{W}_S$ in terms of the chiral angle α_i of the inner tube in the whole series of DWCNTs as

$$\bar{W}_S = -14.13 - 72.93\frac{\alpha_i}{n_i} + 40.36\left(\frac{\alpha_i}{n_i}\right)^2. \tag{16}$$

Such an expression is valid when α_i remains sufficiently small. Here for the inner tube considered as a left handed isomer, α_i is always less than $\pi/6$ (for a right-handed isomer the corresponding α_i value would range between $-\pi/6$ and 0), thus leading to an error which is less that 5%.

B. Chiral discrimination energy

Figure 4 displays the chiral discrimination energy per area unit ΔW_S (meV Å^{-2}) between two DWCNT diastereoisomers $(n_i,m_i)@(n_o,m_o)$ or (l,l) and $(m_i,n_i)@(n_o,m_o)$ or (r,l). Our calculations show that the values of ΔW_S are generally vanishingly small when $\Delta n=n_o-n_i \neq 0$, while the largest values of ΔW_S are obtained when $\Delta n=0$ and $\Delta m=m_o-m_i=9$. Therefore in Fig. 4, we have drawn the series corresponding to these constraints $\Delta n=0$ and $\Delta m=9$ as a function of the inner tube indices (n_i,m_i). We see that the discrimination energy is nearly constant and has the same value around 0.4 meV Å^{-2} for all the n_i series and relatively large m_i values, i.e., large inner radius. On the contrary, the discrimination energy vanishes for small m_i values. Intermediate m_i values lead to a maximum of ΔW_S which is clearly much more enhanced for the series with small n_i values.

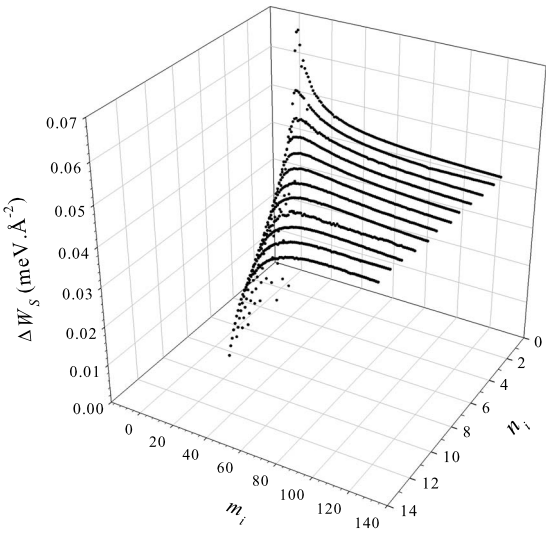

FIG. 4. Discrimination energy ΔW_S between (l,l) and (r,l) DWCNTs vs the integers n_i and m_i defining the inner tube.

We give in Fig. 5 the behavior of the maximum discrimination energy $\Delta W_S^{\max}$ versus inner tube radius R_i, as deduced from the maxima shown in Fig. 4. These maxima display a quasilinear dependence

$$m_i = -5 + 8n_i, \tag{17}$$

as shown in the inset of Fig. 5. The discrimination is maximum and equal to 0.067 meV Å^{-2} for the smallest inner tubes, significantly decreases when R_i increases up to 15 Å, and then very smoothly tends to a finite value for large R_i values. $\Delta W_S^{\max}$ obeys the law

$$\Delta W_S^{\max} = 0.044 + \frac{0.059}{R_i} - \frac{0.017}{R_i^2}. \tag{18}$$

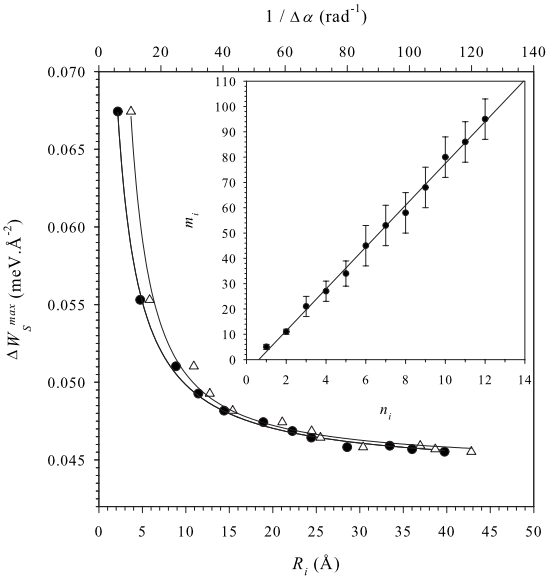

FIG. 5. Maximum discrimination energy $\Delta W_S^{\max}$ between (l,l) and (r,l) DWCNTs vs the inner tube radius R_i (circles) and vs the inverse of the chiral angle difference between the two tubes (triangles). Inset: Linear behavior $n_i(m_i)$ defining the maximum discrimination energy for the series of DWCNTs.

The discrimination energy $\Delta W_S^{\max}$ is positive, in agreement with the fact that two concentric tubes with the same handedness are more stable than their counterpart with different handedness. In Fig. 5, we have also shown the behavior of $\Delta W_S^{\max}$ versus the inverse of the difference $\Delta\alpha = \alpha_i - \alpha_o$ of the chiral angles of the two tubes. This difference can be expressed in terms of R_i, ΔR, and Δn as

$$\Delta\alpha \approx \frac{3d_{CC}n_i}{4\pi R_i}\frac{\Delta R/Ri - \Delta n/n_i}{1 + \Delta R/R_i}. \tag{19}$$

For $\Delta n = 0$, there is no significant difference between the curves $\Delta W_S^{\max}(R_i)$ and $\Delta W_S^{\max}(\Delta\alpha^{-1})$, while the discrimination vanishes as Δn increases (not shown). The behavior of $\Delta W_S^{\max}$ versus $\Delta\alpha^{-1}$ indicates that an increase in the tube radii requires a smaller difference in the chiral angle of the two tubes to keep a maximum chiral discrimination.

To study the influence of the various quantities R, α, and L on the discrimination energy for the two diastereoisomers, we have assumed an outer left-handed tube defined by its characteristics R_o, L_o, and α_o and we have calculated the chiral discrimination energy ΔW_S experienced by a left- or right-handed tube growing inside it, by applying the constraints $R_i = R_o - \Delta R$ and $\alpha_i = \alpha_o R_o / R_i$ (for $\Delta n = 0$) which ensure maximum stability of the DWCNT. The tube characteristics are given in Table I, and Fig. 6 displays the behavior of ΔW_S as a function of the length L_i of the growing tube. For nearly constant values of the radius R_o and length L_o of the outer tube (tubes 1–6 in Table I), an increase in the chiral angle α_o from 1° to 6° induces a strong decrease in ΔW_S when the inner tube length L_i increases up to being equal to that of the outer tube $L_o \approx 777$ Å. The chiral discrimination is, however, maximum for small values of the length L_i, whatever the chiral angle α_o, i.e., at the beginning of the inner tube growth and it favors the (l,l) DWCNT with respect to the (r,l) one.

A small length L_o of the outer tube, concomitantly with a corresponding smaller radius leading to an increase in the chiral angle difference $\Delta\alpha$ and a decrease by a factor 2 of the inner tube radius R_i (tubes 7 and 8 in Table I), is responsible for a decrease in the chiral discrimination. This shows that the discrimination is enhanced when the two tubes have similar chiral angles, since an increase of 1° of $\Delta\alpha$ reduces the discrimination energy between the (l,l) and (r,l) species by about 0.015 meV Å^{-2}. Finally, decreasing by a factor 3 the length L_o of the outer tube without modifying the other characteristics of the two tubes (tubes 8 and 9 in Table I) leads to enhance by the same factor the discrimination energy.

C. Breathing mode frequencies

The behavior of the three force constants k_{Si}, k_{So}, and k_{Sio} used to calculate the breathing mode frequencies of the DWCNTs are shown in Fig. 7 versus the numbers $n_i = 1, \ldots, 9$ and $m_i = n_i + 1, \ldots, 45$. We see that these force constants follow a similar behavior with n_i and with m_i. Their values decrease as m_i increases according to a quadratic polynomial in $1/m_i$ for fixed n_i value, while they increase according to a quadratic polynomial in n_i for fixed m_i. The

TABLE I. Characteristics of DWCNTs used to study ΔW_S vs L_i (Fig. 6).

Fig.[a]	$(n_i,m_i)@(n_o,m_o)$	R_i (Å)	R_o (Å)	α_i (deg)	α_o (deg)	$\Delta\alpha$ (deg)	L_o (Å)
1	(1,36)@(1,45)	14.29	17.81	1.36	1.09	0.27	774
2	(2,36)@(2,45)	14.50	18.02	2.68	2.15	0.52	779
3	(3,35)@(3,44)	14.32	17.84	4.07	3.27	0.80	774
4	(4,34)@(4,43)	14.16	17.67	5.50	4.40	1.10	765
5	(5,35)@(5,44)	14.78	18.28	6.59	5.32	1.27	790
6	(6,35)@(6,45)	15.01	18.51	7.78	6.31	1.48	801
7	(2,16)@(2,25)	6.69	10.20	5.82	3.81	2.04	444
8	(1,8)@(1,17)	3.34	6.86	5.82	2.83	2.98	444
9	(1,8)@(1,17)	3.34	6.86	5.82	2.83	2.98	148

[a]Numbers 1–9 refer to curves drawn in Fig. 6.

values of these force constants decrease as the radii R_i and R_o increase. The smaller value of k_{Sio} found here for a R_i radius equal to 19.7 Å (n_i=8, m_i=45) is 0.048 meV Å^{-4}. It compares very well with the value of k_{Sio} between two graphene sheets (infinite values of R_i and R_o) at the equilibrium distance of 3.51 Å which is equal to 0.046 meV Å^{-4}.

The behavior of the frequencies of the radial breathing modes ω_+ and ω_- versus the tube radius are shown in Fig. 8. These frequencies fit very well with very simple laws

$$\omega_+ = a_+ + \frac{b_+}{R_i}, \tag{20}$$

$$\omega_- = a_- + \frac{b_-}{R_o}, \tag{21}$$

where a_+=10.0 cm^{-1}, b_+=1169.4 cm^{-1} Å, and a_-=−0.6 cm^{-1}, b_-=1236.2 cm^{-1} Å. The values for a_+ and b_+ nicely compare with those determined in Ref. 16(a_+=9 cm^{-1} and b_+=1175 cm^{-1} Å).

The occurrence of points outside the continuous curve is due to the influence of the change in the interwall distance ΔR depending on the tube species. It may be noted that the consideration of this dependence as a polynomial in ΔR in Eqs. (20) and (21) would make all the points being nearly aligned with the curves. In the inset of Fig. 8, we show that introducing a ΔR^2 dependence in the calculated curves of $\omega_\pm$ tends to appreciably reduce the deviation from the ideal curves. This is consistent with the expressions of k_S obtained in the continuum model [Eqs. (A3) and (A4)] when x is approximated by $1-(\Delta R/R_i)^2$ and y_p nearly vanishes for a large value of the inner tube length with respect to the radius (see Appendix).

The chiral influence of the tubes on the breathing modes is shown in Fig. 9. We have drawn the splittings $\Delta\omega_+$ and $\Delta\omega_-$ of the mode frequencies defined as

$$\Delta\omega_\pm = \omega_\pm^{ll} - \omega_\pm^{rl}, \tag{22}$$

as a function of the inner tube radius for ω_+ and of the outer tube one for ω_-. We see that this splitting is generally smaller than 2 cm^{-1}, except for some DWCNTs with interwall distance smaller than 3.4 Å, as shown in the inset of Fig. 9. For such values of ΔR, the interaction between the two tubes

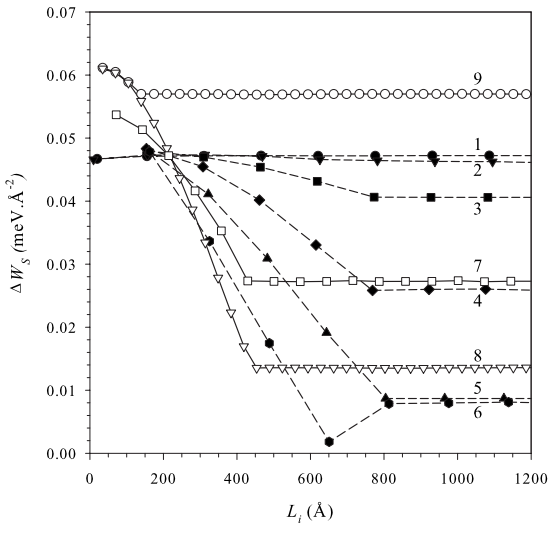

FIG. 6. Chiral discrimination energy for a series of tubes whose characteristics are defined in Table I as a function of the length L_i of the inner tube growing in a consistent outer one. Numbers 1–9 on the curve refer to the values reported in Table I.

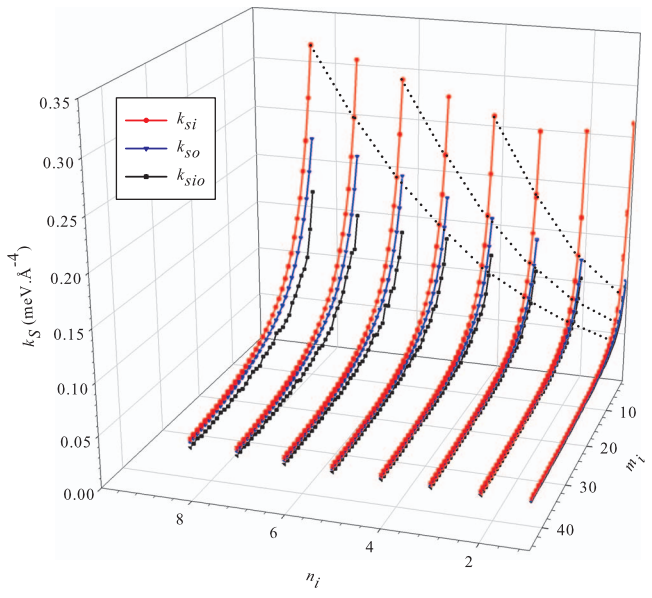

FIG. 7. Behavior of the mean force constants $k_s=(k_S^{ll}+k_S^{rl})/2$ with $k_s=k_{Si}$, k_{So}, and k_{Sio} vs the numbers n_i and m_i for the series of chiral DWCNTs (n_i=1,...,9; $m_i=n_i+1,\ldots,45$). The dotted curves show the behavior of the n_i dependence of k_S for some fixed values of m_i (see the text).

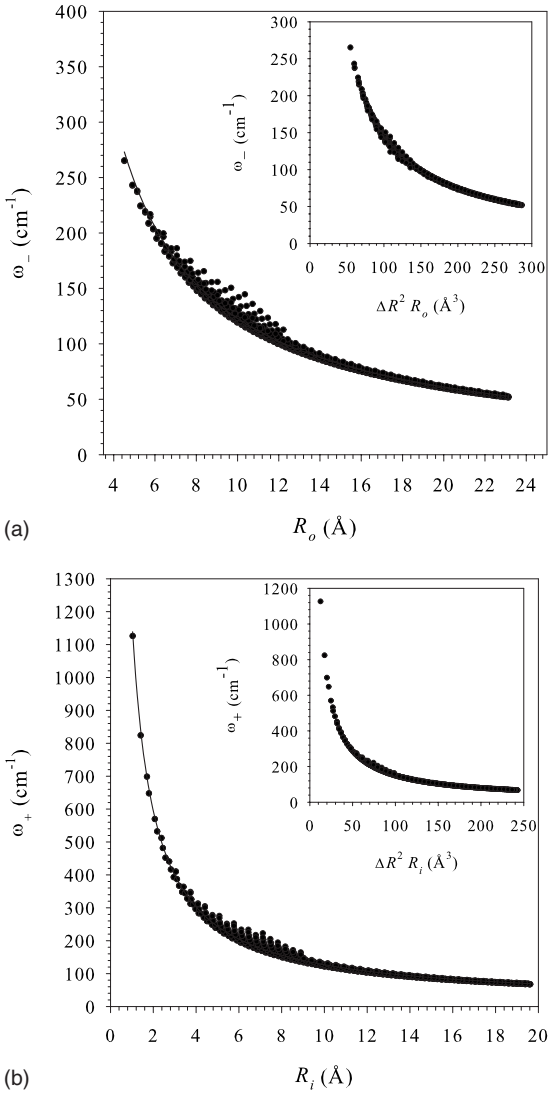

FIG. 8. Behavior of the breathing mode frequencies ω_- (a) and ω_+ (b) (cm^{-1}) vs the radii R_o and R_i, respectively, for the series of chiral DWCNTs. The curves correspond to the fit given in Eqs. (20) and (21).

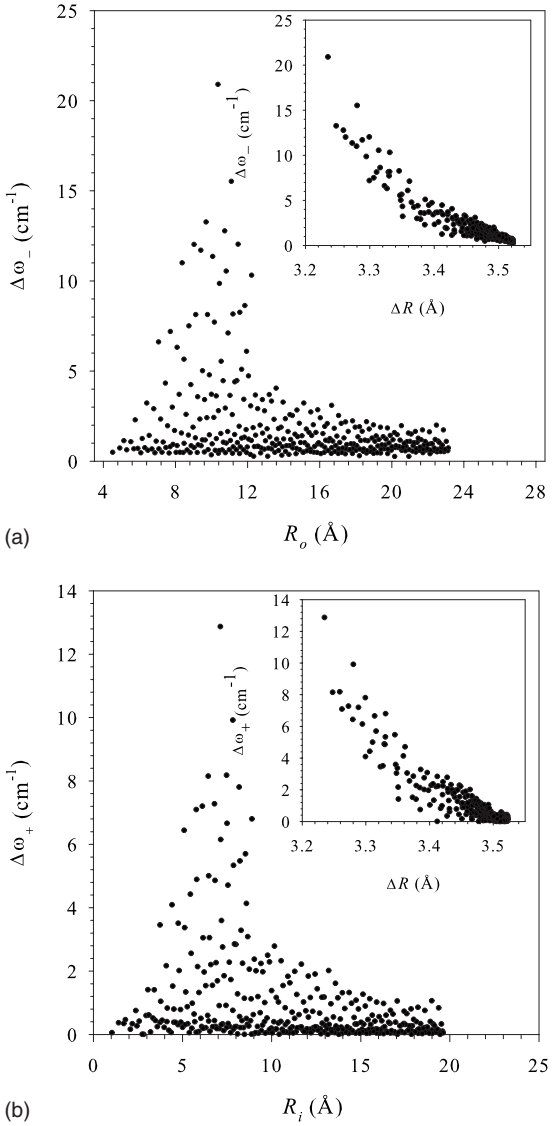

FIG. 9. Frequency splittings $\Delta\omega_-$ (a) and $\Delta\omega_+$ (b) (cm^{-1}) when ((l,l) and (r,l)) DWCNT diastereoisomers are considered vs the tube radii R_o and R_i, respectively. The inset shows the influence of the interwall distance ΔR between the inner and outer tubes on the chiral frequency splitting.

becomes repulsive and the chiral discrimination becomes unrealistically too large, as already mentioned in Sec II.

We give in Fig. 10 the splitting $\Delta\omega_\pm$ of the mode frequencies $\omega_\pm$ corresponding to DWCNTs for which ΔR ranges between 3.4 and 3.6 Å. Since the frequencies decrease as the CNT radius increases [Eqs. (20) and (21)], the strongest splittings (≈ 2 cm^{-1}) are obtained when the chiral angle difference $\Delta\alpha$ ranges between 0.5° and 6° for intermediate values of the inner tube radii (between 5 and 10 Å). Smaller radii ($R_i < 5$ Å) lead to smaller chiral splittings (<1 cm^{-1}) with, however, chiral angle difference values which can reach 10°. In a general way, we see that $\Delta\omega_+$ increases with R_i when α_i is kept constant and with $\Delta\alpha$ when R_i is kept constant. A similar behavior is observed for $\Delta\omega_-$ versus R_o and α_o.

We give in Table II the splittings $\Delta\omega_\pm$ of the frequencies $\omega_\pm$ which are due to the response of the two diastereoisomers $(n_i,m_i)@(n_o,m_o)$ and $(m_i,n_i)@(n_o,m_o)$ for a series of DWCNTs with radii ranging between 2.5 and 4.5 Å. The present results show that chirality can be responsible for splittings in the response ω_+ ($250 \leq \omega_+ \leq 450$ cm^{-1}) of [(l,l) and (l,r)] DWCNTs, which range between -0.5 and $+1$ cm^{-1}, and for splittings in the response ω_- ($140 \leq \omega_- \leq 200$ cm^{-1}) which are generally larger, being between 0.5 and 2 cm^{-1}. The chiral angle difference $\Delta\alpha$ for all these tubes appears to be relatively large since it varies from 2.2° to 12.3°.

IV. DISCUSSION

The interaction between the inner and outer tubes of a DWCNT can be simply expressed as a function of the inner tube radius R_i or chiral angle α_i, when the carbon-carbon interaction is described by a Lennard-Jones potential. The most stable DWCNTs are obtained for small values of R_i and thus of $R_o = R_i + \Delta R$, where ΔR remains close to the interwall distance given by the Lennard-Jones potential. A quasilinear increase in the interaction energy is shown for both (l,l) and (r,l) tubes as R_i increases or α_i/n_i decreases. At small R_i

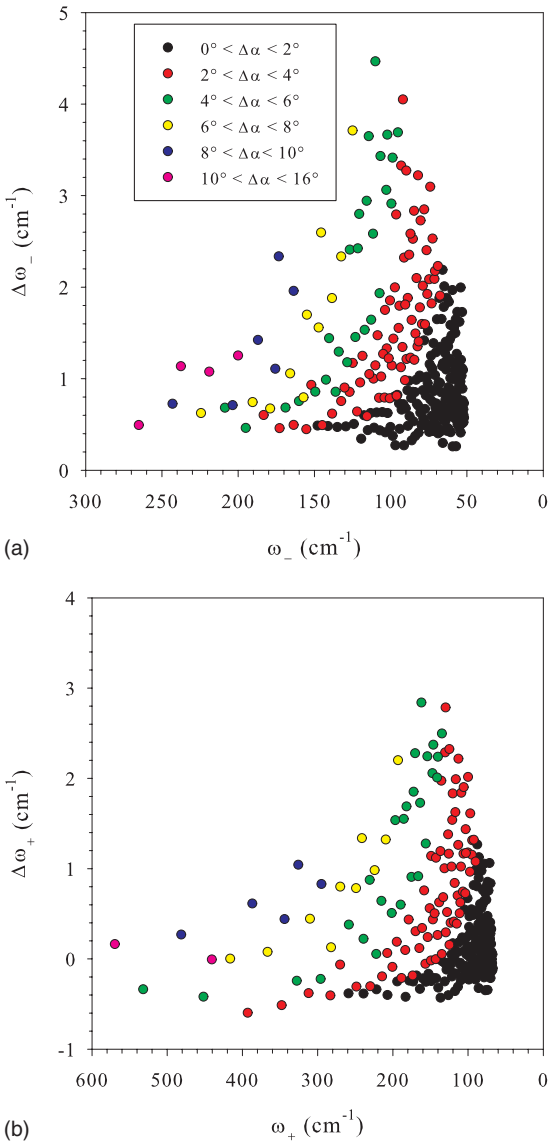

FIG. 10. Frequency splittings $\Delta\omega_-$ (a) and $\Delta\omega_+$ (b) (cm^{-1}) depending on the chiral angle difference $\Delta\alpha=\alpha_i-\alpha_o$ for the (l,l) and (r,l) diastereoisomers.

values, the nonlinear behavior can be interpreted by analyzing the $\Delta R/R_i$ dependence of the analytical expression of the interaction energy written in the continuum model (no chiral effect). The interaction calculated for the two diastereoisomers displays a small chiral discrimination energy as shown by the behavior of ΔW_S with R_i and $\Delta\alpha=\alpha_i-\alpha_o$. For the DWCNT series considered in this paper, the maximum discrimination energy ranges between 0.0675 meV $Å^{-2}$ (0.18 meV/atom) and 0.045 meV $Å^{-2}$ (0.12 meV/atom) when R_i increases from 2.2 to 5.0 Å, or $\Delta\alpha$ increases from 0.5° to 6°. As an example, for a DWCNT with an inner tube characterized by R_i=7 Å and L_i=100 Å, the value of ΔW is 230 meV while $\bar{W}$=68.1 eV.

Though small, it was interesting to see whether this discrimination between (l,l) and (r,l) DWCNTs can influence the mutual growth of the two tubes. We have shown that the chiral discrimination is maximum at the first steps of the growth of the inner tube in the outer one having the same handedness and very similar chiral angles. This maximum value can reach about 0.16 meV/atom, i.e., 6 meV for an inner tube radius of 3.34 Å and a length of 10 Å. This discrimination remains clearly small and it cannot explain by itself the selective growth of DWCNTs having the same handedness, as observed in Ref. 25, but it could participate to this selectivity among other causes.

Since Raman scattering has proven to be a key technique for the analysis of DWCNTs[16,17,23] due to the photoselective resonance response of the radial breathing modes, the behavior of the frequencies of these modes has been examined as a function of the two tubes' radii and of the chiral angle difference for the series of selected tubes. In previous papers,[16,17,23] the splittings of the high resolution Raman frequencies were discussed in terms of the response of one inner tube enclosed in several different outer ones, without regarding the tube chirality. The spectral resolution corresponding to the response of the inner tubes was $\approx$0.35 cm^{-1}. Splittings between -2 and +2 cm^{-1} around the mean frequency values were observed for inner tubes with radii ranging between 2.5 and 4.5 Å.

The corresponding splittings calculated in Table II correspond precisely to the set of DWCNTs studied in Refs. 17 and 23. Note, however, that some of them occurring in these references are not stable in our calculations (ΔR interwall distance less than 3.4 Å) and they have been removed from Table II. For ω_+, the splitting assigned to the chirality lies in a smaller extent than the one assigned to the filling of several larger outer tubes by a given inner one. However, since the interaction energy of these diastereoisomers is *a priori* more stable than the energy between tubes with larger interwall distances, these chiral splittings, which are at the limit of detection, should be taken into account to interpret the Raman spectrum. Note that the frequency splittings due to chirality are generally larger for the outer tubes (reaching 2 cm^{-1}) than for the inner ones, but the experimental resolution is in this case less good[17] and it would prevent their observation. It may be noted that all the calculations have been performed with the theoretical values of the radius and the chiral angle of the tubes obtained from Eqs. (2) and (3). The values of the radii deduced from density functional theory[17] are generally larger than these theoretical values, leading to slightly smaller values of the breathing mode frequencies. But this correction should not strongly affect the splitting values determined here.

V. CONCLUSION

Chirality in nanotubes has been and is still the subject of intensive research since it can be responsible for unique properties leading to technological applications in photoelectronics, quantum optics, and biosensor devices, for instance. To our knowledge, no quantitative data were available on the influence of chirality on the stabilization energy and vibration of DWCNTs formed by two left-handed concentric tubes or one left-handed and the other right-handed tube. A large sampling of DWCNT diastereoisomers has been used to deduce simple laws on the chiral energy discrimination and on the chiral splitting of the breathing mode frequencies. Although chiral effects generally remain weak, they influence

TABLE II. Chiral splittings $\Delta\omega_{\pm}$ (cm^{-1}) of the breathing mode frequencies $\omega_{\pm}$ (cm^{-1}) for DWCNTs with inner radius values ranging between 2.5 and 4.5 Å. The chiral angle difference $\Delta\alpha$ is given for each DWCNT.

$(n_i,m_i)@(n_o,m_o)$	ω_-	$\Delta\omega_-$	ω_+	$\Delta\omega_+$	$\Delta\alpha$ (deg)
(1,6)@(1,15)	195.05	0.46	451.85	−0.42	4.4
(3,5)@(3,14)	200.05	1.25	440.74	−0.01	12.3
(2,6)@(2,15)	190.51	0.74	416.22	0.00	7.7
(1,7)@(1,16)	183.33	0.60	392.89	−0.60	3.6
(3,6)@(3,15)	187.02	1.42	386.86	0.61	10.2
(2,7)@(2,16)	179.03	0.67	366.57	0.08	6.4
(1,8)@(1,17)	172.83	0.46	347.80	−0.51	3.0
(3,7)@(3,16)	175.64	1.11	344.09	0.44	8.6
(2,8)@(2,17)	169.00	0.68	327.70	−0.24	5.4
(4,7)@(4,16)	173.41	2.34	325.70	1.04	10.2
(1,9)@(1,18)	163.66	0.49	311.98	−0.38	2.5
(3,8)@(3,17)	165.89	1.06	310.15	0.44	7.3
(2,9)@(2,18)	160.15	0.75	295.99	−0.22	4.6
(4,8)@(4,17)	163.63	1.96	295.02	0.83	8.8
(1,10)@(1,19)	155.34	0.45	283.06	−0.41	2.2
(3,9)@(3,18)	157.18	0.80	282.24	0.13	6.3
(2,10)@(2,19)	152.05	0.93	270.09	−0.06	4.0
(4,9)@(4,18)	154.97	1.70	270.02	0.80	7.7
(3,10)@(3,19)	149.48	0.86	258.57	0.38	5.5
(3,11)@(3,20)	142.47	0.99	238.97	0.22	4.9

the stabilization energy of the two tubes and they give additional signals in the high resolution Raman spectrum that should be experimentally detected. In terms of interaction energy and of spectral response, chirality in nanotubes appears to be a short range phenomenon; i.e., its effect is maximum when the interwall distance is close to the equilibrium value. It is also an intrinsic property of the two coaxial tubes and therefore its influence should be described in similar terms step by step from an inner tube to an outer one. It is therefore expected that the present results, which apply to any size and chiral angle of CNTs, could be easily extended to the analysis of the MWCNT chirality.

APPENDIX: INTERACTION POTENTIAL AND FORCE CONSTANTS IN THE CONTINUUM MODEL

In the potential defined by Eq. (11), $x=4R_iR_o/(R_i+R_o)^2$ and $y_p=4R_iR_o/[(R_i+R_o)^2+\Lambda_p^2]$ are adimensional variables depending on the inner and outer tube radii and on the lengths $\Lambda_1=(L_o+L_i)/2$ and $\Lambda_2=(L_o-L_i)/2$. The functions $N_6(x,y_p)$ and $N_{12}(x,y_p)$ are expressed in terms of the hypergeometric Appell functions[35] $F_1(n',n'',n''',n'''',x,y_p)$ as

$$N_6(x,y_p)=\frac{(-)^{p+1}}{\Lambda_p^2}(x-y_p)\left(3\sum_{k=0}^{\infty}\frac{(2k)!}{2^{2k}(k!)^2(2k+1)\Lambda_p^{k+1}}\frac{(x-y_p)^{k+1}}{y_p^{3/2}x^{k-1/2}}F_1(1/2,5/2,k+1/2,1,x,y_p)-F_1(1/2,1,1,1,x,y_p)\right), \tag{A1}$$

$$N_{12}(x,y_p)=\frac{1}{32}\frac{(-)^{p+1}}{\Lambda_p^8}(x-y_p)^4\left(63\sum_{k=0}^{\infty}\frac{(2k)!}{2^{2k}(k!)^2(2k+1)\Lambda_p^{k+1}}\frac{(x-y_p)^{k+1}}{y_p^{9/2}x^{k-1/2}}F_1(1/2,11/2,k+1/2,1,x,y_p)-\frac{21}{y_p^3}F_1(1/2,4,1,1,x,y_p)\right.$$
$$\left.-\frac{8.4}{xy_p^2}F_1(1/2,3,2,1,x,y_p)-\frac{4.8}{x^2y_p}F_1(1/2,2,3,1,x,y_p)-\frac{3.2}{x^3}F_1(1/2,1,4,1,x,y_p)\right). \tag{A2}$$

The force constants determined from the continuum model [Eq. (11)] are defined as

$$k_{Si}=\frac{2.921}{2\pi R_iL_od_{CC}^4R_i^2}\sum_{k=6,12}(-)^{k/2}C_k\sum_{p=1}^{2}\left\{x^2\left[x^{-1/2}\left(\frac{R_o}{R_i}\right)^{1/2}-\frac{3}{2}\right]\frac{\partial N_k}{\partial x}-y_p^2\frac{R_i}{R_o}\left[\frac{1}{2}+2x^{-1/2}\left(\frac{R_o}{R_i}\right)^{1/2}-2x^{-1}y_p\right]\frac{\partial N_k}{\partial y_p}+x^2[1-x]\frac{\partial^2N_k}{\partial x^2}\right.$$
$$\left.+y_p^2\left[1-y_px^{-1/2}\left(\frac{R_i}{R_o}\right)^{1/2}\right]^2\frac{\partial^2N_k}{\partial y_p^2}+2xy_p\left[1-x^{-1/2}y_p\left(\frac{R_i}{R_o}\right)^{1/2}\right]\left[1-x^{1/2}\left(\frac{R_i}{R_o}\right)^{1/2}\right]\frac{\partial^2N_k}{\partial x\,\partial y_p}\right\} \tag{A3}$$

and

$$k_{Sio} = \frac{2.921}{2\pi R_i L_o d_{CC}^4 R_i R_o} \sum_{k=6,12} (-)^{k/2} C_k \sum_{p=1}^{2} \left\{ x\left[\frac{3}{2}x - 1\right]\frac{\partial N_k}{\partial x} + y_p\left[1 - \frac{y_p}{2} + 2y_p x^{-1}(y_p - 1)\right]\frac{\partial N_k}{\partial y_p} \right.$$
$$\left. + x^2[x-1]\frac{\partial^2 N_k}{\partial x^2} + y_p^2[1 + y_p^2 x^{-1} - 2y_p x^{-1}]\frac{\partial^2 N_k}{\partial y_p^2} + y_p\left[2x + 2y - \frac{1}{2}x^{-1}(1+y)\right]\frac{\partial^2 N_k}{\partial x\,\partial y_p}\right\}. \quad \text{(A4)}$$

The third force constant k_{So} can be obtained from Eq. (A3) by permuting R_i and R_o, x and y_p being invariant in this permutation.

[1] R. Saito, G. Dresselhaus, and M. S. Dresselhaus, *Physical Properties of Carbon Nanotubes* (Imperial College Press, London, 1998).
[2] R. A. Jishi, M. S. Dresselhaus, and G. Dresselhaus, Phys. Rev. B **47**, 16671 (1993).
[3] N. Komatsu, J. Inclusion Phenom. Macrocyclic Chem. **61**, 195 (2008).
[4] X. Huang, R. S. Mclean, and M. Zheng, Anal. Chem. **77**, 6225 (2005).
[5] G. Dukovic, M. Balaz, P. Doak, N. D. Berova, M. Zheng, R. S. Mclean, and L. E. Brus, J. Am. Chem. Soc. **128**, 9004 (2006).
[6] M. S. Strano, Nat. Nanotechnol. **2**, 340 (2007).
[7] M. Zheng and E. D. Semke, J. Am. Chem. Soc. **129**, 6084 (2007).
[8] X. Peng, N. Komatsu, T. Kimura, and A. Osuka, ACS Nano **2**, 2045 (2008).
[9] H. Zhu, K. Suenaga, J. Wei, K. Wang, and D. Wu, J. Cryst. Growth **310**, 5473 (2008).
[10] X. Peng, N. Komatsu, T. Kimura, and A. Osuka, J. Am. Chem. Soc. **129**, 15947 (2007).
[11] A. Green, M. Duch, and M. Hersam, Nano. Res. **2**, 69 (2009).
[12] T. Sugai, H. Yoshida, T. Shimada, T. Okazaki, H. Shinohara, and S. Bandow, Nano Lett. **3**, 769 (2003).
[13] E. Flahaut, C. Laurent, and A. Peigney, Carbon **43**, 375 (2005).
[14] P. Ramesh, T. Okazaki, R. Taniguchi, J. Kimura, T. Sugai, K. Sato, Y. Ozeki, and H. Shinohara, J. Phys. Chem. B **109**, 1141 (2005).
[15] S. Bandow, G. Chen, G. U. Sumanasekera, R. Gupta, M. Yudasaka, S. Iijima, and P. C. Eklund, J. Am. Chem. Soc. **66**, 075416 (2002).
[16] R. Pfeiffer, H. Kuzmany, C. Kramberger, C. Schaman, T. Pichler, H. Kataura, Y. Achiba, J. Kürti, and V. Zólyomi, Phys. Rev. Lett. **90**, 225501 (2003).
[17] C. Kramberger, R. Pfeiffer, H. Kuzmany, V. Zólyomi, and J. Kürti, Phys. Rev. B **68**, 235404 (2003).
[18] J. Wei, B. Jiang, X. Zhang, H. Zhu, and D. Wu, Chem. Phys. Lett. **376**, 753 (2003).
[19] M. Kociak, K. Hirahara, K. Suenaga, and S. Iijima, Eur. Phys. J. B **32**, 457 (2003).
[20] K. Hirahara, M. Kociak, S. Bandow, T. Nakahira, K. Itoh, Y. Saito, and S. Iijima, Phys. Rev. B **73**, 195420 (2006).
[21] C. E. Giusca, Y. Tison, V. Stolojan, E. Borowiak-Palen, and S. R. P. Silva, Nano Lett. **7**, 1232 (2007).
[22] R. Saito, R. Matsuo, T. Kimura, G. Dresselhaus, and M. S. Dresselhaus, Chem. Phys. Lett. **348**, 187 (2001).
[23] R. Pfeiffer, C. Kramberger, F. Simon, H. Kuzmany, V. Popov, and H. Kataura, Eur. Phys. J. B **42**, 345 (2004).
[24] M. Xia, S. Zhang, X. Zuo, E. Zhang, S. Zhao, J. Li, L. Zhang, Y. Liu, and R. Liang, Phys. Rev. B **70**, 205428 (2004).
[25] Z. Liu, K. Suenaga, H. Yoshida, T. Sugai, H. Shinohara, and S. Iijima, Phys. Rev. Lett. **95**, 187406 (2005).
[26] A. V. Belikov, Y. E. Lozovik, A. G. Nikolaev, and A. M. Popov, Chem. Phys. Lett. **385**, 72 (2004).
[27] L. Bellarosa, E. Bakalis, M. Melle-Franco, and F. Zerbetto, Nano Lett. **6**, 1950 (2006).
[28] E. Bakalis and F. Zerbetto, Chem. Phys. Lett. **463**, 139 (2008).
[29] L. Guan, K. Suenaga, and S. Iijima, Nano Lett. **8**, 459 (2008).
[30] G. Román-Pérez and J. M. Soler, Phys. Rev. Lett. **103**, 096102 (2009).
[31] L. Ci, Z. Rao, Z. Zhou, D. Tang, X. Yan, Y. Liang, D. Liu, H. Yuan, W. Zhou, G. Wang, W. Liu, and S. Xie, Chem. Phys. Lett. **359**, 63 (2002).
[32] The corresponding energy expressed in meV/atom can be obtained using the conversion rule: 1 meV $Å^{-2}$=2.63 meV/atom.
[33] J. Breton, J. Gonzalez-Platas, and C. Girardet, J. Chem. Phys. **101**, 3334 (1994).
[34] D. Cao and W. Wang, Eng. Sci. **62**, 6879 (2007).
[35] D. Baowan and J. M. Hill, Z. Angew. Math. Phys. **58**, 857 (2007).
[36] E. Dobardzic, J. Maultzsch, I. Milosevic, C. Thomsen, and M. Damnjanovic, Phys. Status Solidi B **237**, R7 (2003).